Optimization of Intensities and Locations of Diffuse Spots in Indoor Optical Wireless Communications

Mahmoud W. Eltokhey[a,b], Korany R. Mahmoud[a,c], Zabih Ghassemlooy[d,e], S. S. A. Obayya[a]

[a] Centre for Photonics and Smart Materials, Zewail City of Science and Technology, Giza 12588, Egypt

[b] Institut Fresnel, UMR CNRS 7249, Ecole Centrale Marseille, Marseille, France

[c] Electronics, Communications and Computers Department, Faculty of Engineering, Helwan University, Cairo, Egypt

[d] Optical Communications Research Group, NCRLab, Faculty of Engineering and Environment, Northumbria University, Newcastle upon Tyne, NE1 8ST, UK

[e] QIEM, Haixi Institutes, Chinese Academy of Sciences, Quanzhou, China

***Abstract*— In this paper, optimization of diffuse spots' parameters in indoor optical wireless communications (OWC) system is carried out by using the particle swarm optimization (PSO) algorithm. By simultaneously optimizing the diffusion spots' locations and intensities, we show an improvement in the signal-to noise-ratio (SNR) and the delay spread at the receivers, while considering both the background noise and the multipath dispersion. A comparison is made between different optimization scenarios, to illustrate the effect of varying the parameters that are being optimized. We show that the optimization of both intensities and locations of diffuse spots resulted in improvement up to 42% and 23% in the average delay spread and the average SNR, respectively, compared with the centrally located position of diffuse spots' distribution, with respect to the receivers' locations, which has a uniform distribution of power.**

Keywords—Optical wireless communications; indoor communications; particle swarm optimization; optimization.

I. INTRODUCTION

The un-regulated optical wireless communications (OWC) systems offer high transmission bandwidth, inherent security, not being affected by radio frequency based interference, and the ability to use the same wavelength (frequency) within a room or an entire building [1, 2]. These advantages make OWC an attractive and complementary candidate to the radio frequency based wireless technologies in a number of applications such as intravehicle communications [3], wireless sensor networks [4], healthcare monitoring [3,5], and others [3]. However, in line with other communications technologies, in OWC systems there are a number of issues such as (*i*) eye and skin safety which limits the transmitted optical power; (*ii*) multipath induced intersymbol interference in non-line of sight (LOS) environments, which leads to reduced bit error rate (BER) performance [6,7]; (*iii*) the ambient lights' noise which degrades the SNR performance [8, 9]; (*iv*) shadowing and lack of mobility in LOS configurations in contrast to non-LOS links [3,6].

In order to improve the OWC system performance, optimization of the key parameters based on different approaches have been studied in the literature. In [10], the use of genetic algorithm for controlling the optical wireless channel was proposed. However, the authors did not consider the delay spread (DS) in the fitness function. In [11] and [12] divide and conquer algorithm was used for sequentially adapting different transmitters' (Tx's) parameters in an indoor OWC environment. Simulated annealing adopted in [13] showed improvement in the average DS and the standard deviation of the received power by optimizing the spot pattern in diffuse OWC links, however, the spots' intensities were not considered. In [14] optimization of the center of diffuse spots' distribution was considered, but not the intensities of the diffuse spots (DiSs).

In this work, particle swarm optimization (PSO) technique is used for finding optimized distribution for the locations and the intensities of the diffusion spots, considering simultaneously maximizing the SNR and minimizing the delay spread at the users, while taking into account the effects of background noise and multipath dispersion. In addition, a comparison is carried out between different optimization scenarios, considering different variables in the optimization, in order to illustrate the impact of changing the optimization parameters on the system performance. The results obtained are compared with the data based on the central located positions, with respect to the Rxs' locations, of a circular distribution of equal intensities diffusion spots. The channel model and the optimization algorithm developed can be generalized for almost any indoor diffuse OWC based local area networks (LAN), with randomly placed Txs and Rxs.

The remainder of the paper is structured as follows. In Section 2 a description for the OWC system model and the

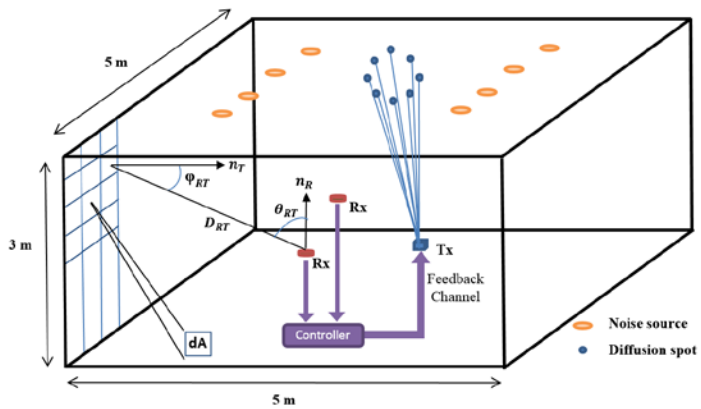

Fig. 1. Illustration of the indoor OWC environment considered in this work

channel characteristics is provided. In Section 3 a brief description for the PSO optimization technique is provided. Results and discussion of the results are provided in Section 4. The conclusion is presented in Section 5.

II. OWC System Model

Here, we consider a typical indoor environment, see Fig. 1, which is composed of a Tx, Rxs, noise sources, and a feedback channel. A single Tx (2-D vertical cavity surface emitting laser diode or resonant cavity LED array [10, 15, 16]) can be used to project DiSs onto the ceiling, which are considered as secondary independent Txs. Note that, it is possible to project diffuse patterns depending on the room shape and size and its use. The feedback path provides the Tx with relevant information, in order to change both locations and intensities of the DiSs.

Note that, the DiSs are considered as Lambertian reflectors [1], with a reflection coefficient of ρ, and only the 1st and the 2nd order reflections are considered, as higher order reflections have negligible contributions [1], [8], [9]. The channel impulse response is given as [9]:

$$h(t;T_F;R_F)=\sum_{r=0}^{k}h^r(t;\mathcal{T};\mathcal{R}) \quad (1)$$

$$h^r(t;\mathcal{T};\mathcal{R})=P_S\sum_{m=1}^{N_e}\frac{L+1}{2\pi}\frac{cos^L(\varphi_{RT})\cos(\theta_{RT})}{{D^2}_{RT}}\rho A_R \times rect\left(\frac{\theta_{RT}}{FOV_R}\right)\delta\left(t-\frac{D_{RT}}{c}\right) \quad (2)$$

where L is the Lambertian order, P_S is the transmitted power. T_F and R_F are the first transmitting and the final receiving points, respectively, and t and the delta function refer to the time of receiving the impulse response component at the Rx, but after taking into consideration that the unit impulse is radiated at $t = 0$ [10]. r is the reflection order of the impulse response, where $r = 0$ refers to the LOS component, and N_e is the number of reflecting elements. T is the point acting as a secondary Tx, which can be a diffusion spot or a Lambertian reflecting surface. R refers to receiving points, which may be a photodetector (PD) or a reflecting surface. $h^r(t;\mathcal{T};\mathcal{R})$ is the r^{th} reflection order impulse response. D_{RT} is the distance between the receiving point and the transmitting point, and A_R is the photosensitive surface area or the area of a reflecting element. FOV_R is the field of view of the PD, which equals 170◦. When the receiving point is a reflecting element, the term which contains FOV_R equals 1. For $x \leq 1$, the $rect(x) = 1$, otherwise is zero. θ_{RT} refers to the angle between D_{RT} and normal to the receving point n_R, and φ_{RT} is the the angle between D_{RT} and normal to the transmitting point n_T. c is the speed of light.

For an intensity modulation direct detection (IM/DD) OWC system, the received photocurrent is given by [17]:

$$y(t)=RPD\;x(t)*\;h(t;T_F;R_F)+n(t) \quad (3)$$

where RPD refers to the responsivity of the PD, $x(t)$ is the transmitted signal, and $n(t)$ is the additive white Gaussian noise. The DS is given by [18]:

$$\mathrm{DS}=\sqrt{\frac{\int(\mathrm{t}-\mu)^2(h(t;\mathrm{T_F};\mathrm{R_F}))^2\mathrm{dt}}{\int(h(t;\mathrm{T_F};\mathrm{R_F}))^2\mathrm{dt}}} \quad (4)$$

where μ is the mean delay, which is given by:

$$\mu=\frac{\int t\,(h(t;\mathrm{T_F};\mathrm{R_F}))^2dt}{\int\,(h(t;\mathrm{T_F};\mathrm{R_F}))^2dt} \quad (5)$$

For on-off keying (OOK) non-return to zero (NRZ) IM/DD OWC, the SNR is given by [8]:

$$\mathrm{SNR}=\frac{(RPDP_r)^2}{{\sigma^2}_{\mathrm{total}}} \quad (6)$$

where P_r is the average optical received power, and ${\sigma^2}_{\mathrm{total}}$ is the total variance of the noise, which is given as:

$${\sigma^2}_{\mathrm{total}}={\sigma^2}_{\mathrm{PA}}+{\sigma^2}_{\mathrm{BN}} \quad (7)$$

where ${\sigma^2}_{PA}$ is the noise variance of the preamplifier, which is the same as the one used in [19]. ${\sigma^2}_{BN}$ is the ambient lights' noise variance given by [20]:

$${\sigma^2}_{\mathrm{BN}}=2\mathrm{q}\mathrm{R_R}\,\mathrm{P_{bn}}\mathrm{BW} \quad (8)$$

Where q is the electron charge, P_{bn} is the ambient lights' power, and BW is the bandwidth of the Rx.

III. Particle Swarm Optimization

The PSO algorithm is considered a stochastic optimization technique, which is based on movement of swarms [21]. It has been shown in literature that particle swarm optimization (PSO) outperforms different optimization techniques, such as genetic algorithm (GA) [22, 23] when tested over different problems. The solution in PSO is a point located in the search space, which is referred to as the particle. All the particles move in the solution space, which has D-dimensions (D is the number of variables in the problem), effected in choosing their new locations by the best position achieved by each particle Pbest, and by all the particles Gbest. For explaining the PSO algorithm, imagine a swarm of bees flying in a field containing flowers, and searching for locations with highest density of flowers. Each bee begins its search by exploring random locations, and communicating to the other bees where the best location in terms of flower density is found. Following this, the bees update their directions and velocities for finding the best locations, influenced by each bee's personal best position, and by the global best position achieved by all the bees. The bees correspond to the particles in the solution space of PSO, such that each particle refers to a solution. The field containing flowers corresponds to the solution space. The density of the flowers represents the solution's fitness value, such that larger densities of flowers corresponds to larger fitness values. For the i[th] particle, the position and the velocity vectors $\mathbf{X_i}$ = (x_{i1}, x_{i2},….,x_{iD}), and $\mathbf{V_i}$ = (v_{i1}, v_{i2}, . . . , v_{iD}), respectively, are updated at every iteration in PSO. In addition, the personal best position P_{besti} = (p_{besti1}, p_{besti2},…,p_{bestiD}), and the global best position G_{best} achieved by all the particles are updated in every iteration. For the i^{th} particle, at the k+1 iteration, the velocity is given by:

$$v_{id}^{k+1} = w^k v_{id}^k + c_1^k rand_1\left(pbest_{id} - x_{id}^k\right) + c_2^k rand_2\left(gbest_d - x_{id}^k\right) \quad (9)$$

And the new position is given by:

$$x_{id}^{k+1} = x_{id}^k + v_{id}^k \Delta t \quad (10)$$

where w^k (within the range of 0.9 to 0.4 [24]) refers to the inertia weight, which is used to control contributions from previous velocities to new velocities. c_1^k and c_2^k are the weights (varied from 2.5 to 0.5 and from 0.5 to 2.5, respectively [25]) which control the influence of P_{best} and G_{best} on the new velocity. $rand_1$ and $rand_2$ are random numbers in the range of 0 and 1. Δt is considered to be equal to unit time step. Here, we have considered hard boundary conditions for controlling the errant probes. Regarding the time complexity of PSO, it has been shown in literature that PSO has lower complexity than other algorithms such as GA [26]. More details about PSO can be found in [21]. Figure 2 shows a flow chart for the considered PSO algorithm.

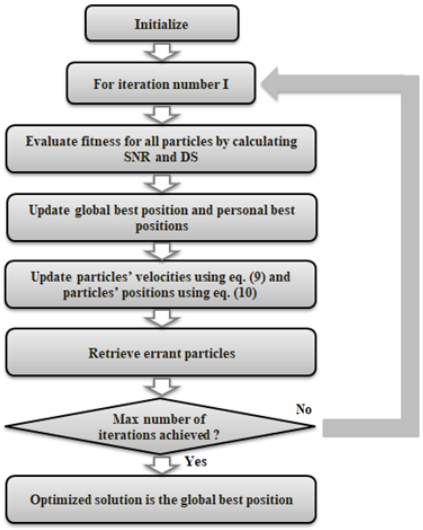

Fig. 2. Flowchart for the considered PSO algorithm

IV. Results and Discussions

In this work, we consider in our simulations a typical indoor environment with dimensions of 5 m × 5 m × 3 m (length × width × height). 4 Rxs are randomly located at 1 m above the floor level, whereas 8 Philips PAR 38 Economic (PAR38) light emitting diode lights, with a Lambertian order of 33.1, and emitted power of 65 W, are considered as the noise sources [27]. It should be noted that the noise sources are more directive than the diffuse spots, because of their Lambertian order. The 8 diffuse spots acting as secondary Txs are considered as independent sources. For the first optimization scenario (Scenario 1), the 8 DiSs are distributed uniformly in a circle of a 0.5 m radius, whereas for the second optimization scenario (Scenario 2) DiSs are randomly distributed. For both scenarios, the DiSs intensities are non-uniform and are randomly distributed but with a total emitted power of 1 W. Table 1 shows all the key simulation parameters considered in this work. Note that, the choice of the adopted data rate is subject to many considerations such as the system complexity, and the scope of the work. Higher data rates can be investigated by considering different components as part of the future work. The diffuse optical wireless communications has been considered in different applications such as wireless sensor networks [4] and healthcare applications [28].

TABLE 1. KEY SIMULATION PARAMETERS

Parameter	Value
PSO algorithm - Total evaluations - No. of iterations - No. of particles	 500 [15] 50 10
Room dimension	(5m length × 5m width × 3m height)
Reflectivity of walls	0.8
Reflectivity of ceiling	0.8
Reflectivity of floor	0.3
Receivers' locations	(1.6,2.1,1), (4.8,4.5,1), (3.3,0.7,1), and (0.4, 2.2,1)
Noise sources' locations	(1,1,3), (1,2,3), (1,3,3), (1,4,3), (4,1,3), (4,2,3), (4,3,3), and (4,4,3)
Photodetector (PIN) responsivity	0.5 A/W
Bit rate	50 Mbps
Receiver bandwidth	70 MHz

The possible values for the locations are within the range of 0.6 m and 4.4 m, to make sure that the optimized locations of DiSs are not close to the corners of the room. The possible values for intensities of the optimized DiSs are in the range of 0.05 W - 0.125 W, such that the intensity of the 8th diffuse spot is equal to the difference between the total power and the intensities of the remaining 7 DiSs. For each evaluation in the optimization process, the intensities of the first 7 DiSs are varied within the allowed range according to the optimization algorithm's results. After defining the intensities of the first 7 DiSs, the intensity of the 8th diffuse spot is equal to the amount which makes the summation of the intensities of the DiSs equal to 1 Watt. The DiSs' intensities could be varied by flip-chip bonding of the sources of the DiSs to CMOS driver circuitry [10, 15, 16]. For maximizing and minimizing the SNR and the delay spread at the Rxs, respectively, while accounting for the reflections and the indoor noise sources, we

have used the following fitness function throughout the optimization process:

$$F = \sum_{k=1}^{N_R} (\omega_1 \times \mathrm{SNR}_k - \omega_2 \times DS_k) \quad (11)$$

where N_R is the total number of Rxs, SNR_k and DS_k are the SNR and the delay spread for the k^{th} Rx, respectively. $\omega_1 = 1, \text{and } \omega_2 = 1 \times 10^9$ are the weights, which control contributions from each term to the objective function. It should be noted that the delay spread is considered in the fitness function as it could affect the bit rate and the BW at the Rxs. Note that, the time complexity of the considered PSO algorithm is defined by $O(N_{IT} \times N_P \times D)$, where N_{IT} is the maximum number of iterations and N_P is the total number of particles. In addition, The space complexity of PSO is equal to $O(N_P \times D)$ [29].

According to the designed algorithm, the PSO algorithm will work on checking continuously the performance at the Rxs, and adapting the diffusion spots' locations and intensities according to the detected performance at receivers. By looking at the fast pace movement speed in indoor environments (about 0.5 m/second [30]), the PSO algorithm should need relaxed conditions, such as checking the performance at the receivers every 0.25 second, for adapting the diffusion spots according to the performance for the users, which is achievable using the considered number of PSO evaluations. For increasing the speed of PSO convergence, the last achieved optimum configuration for the diffusion spots could be forwarded as an initial condition for PSO.

Figures 3 and 4 show the optimized values for the locations and intensities of DiSs for Scenarios 1 and 2, respectively. Also shown are the locations of the Rxs and the noise sources. The number of variables adopted for optimization are 10 for Scenario 1 (2 and 8 for locations and intensities of the DiSs, respectively) and 24 for Scenario 2 (16 and 8 for locations and intensities of the DiSs, respectively). As shown in Figure 3(a), the optimized locations are distributed close to the Rxs 1 and 4, which are most affected by the noise sources. Note that, the Rxs 2 and 3 suffer less from the noise sources, since they are close to only one of the noise source. As depicted in Figure 3(b) the distribution of intensities displays a very high power for S8 compared to the other DiSs. This is because S8 can serve two Rxs 1 and 3, with the Rx3 being too far away, thus the need for higher transmit

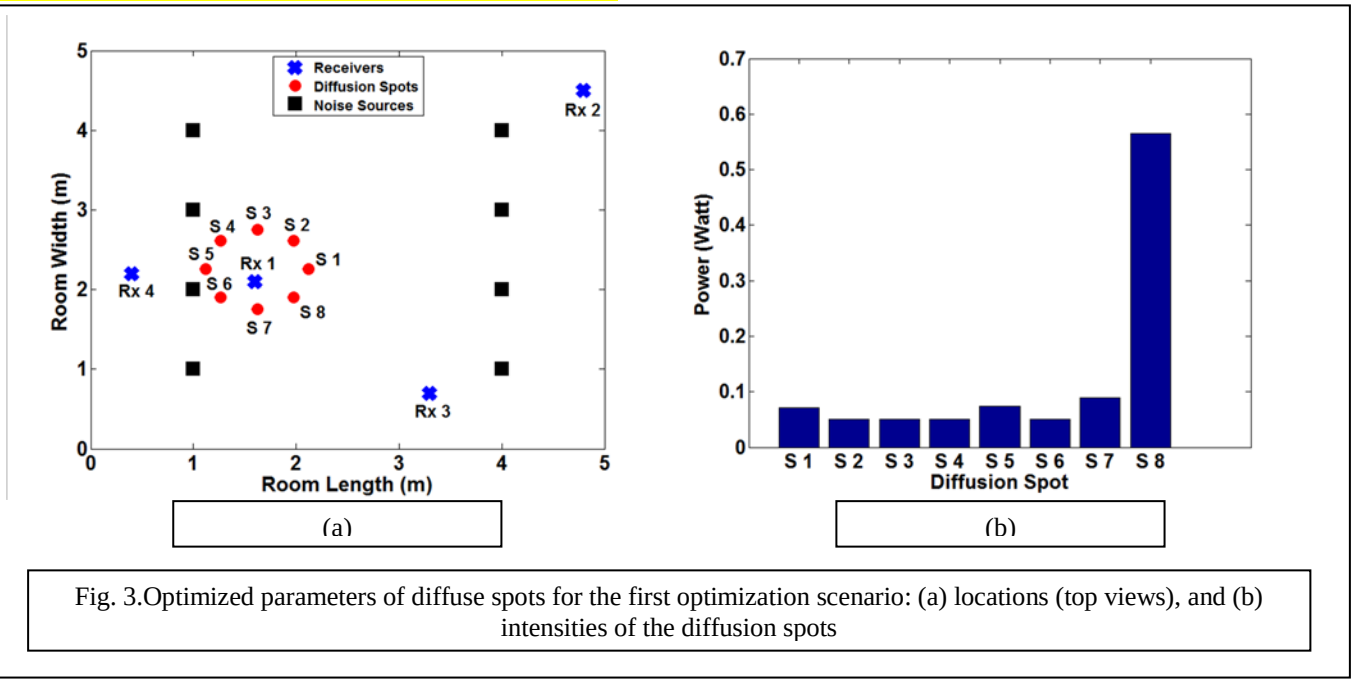

Fig. 3.Optimized parameters of diffuse spots for the first optimization scenario: (a) locations (top views), and (b) intensities of the diffusion spots

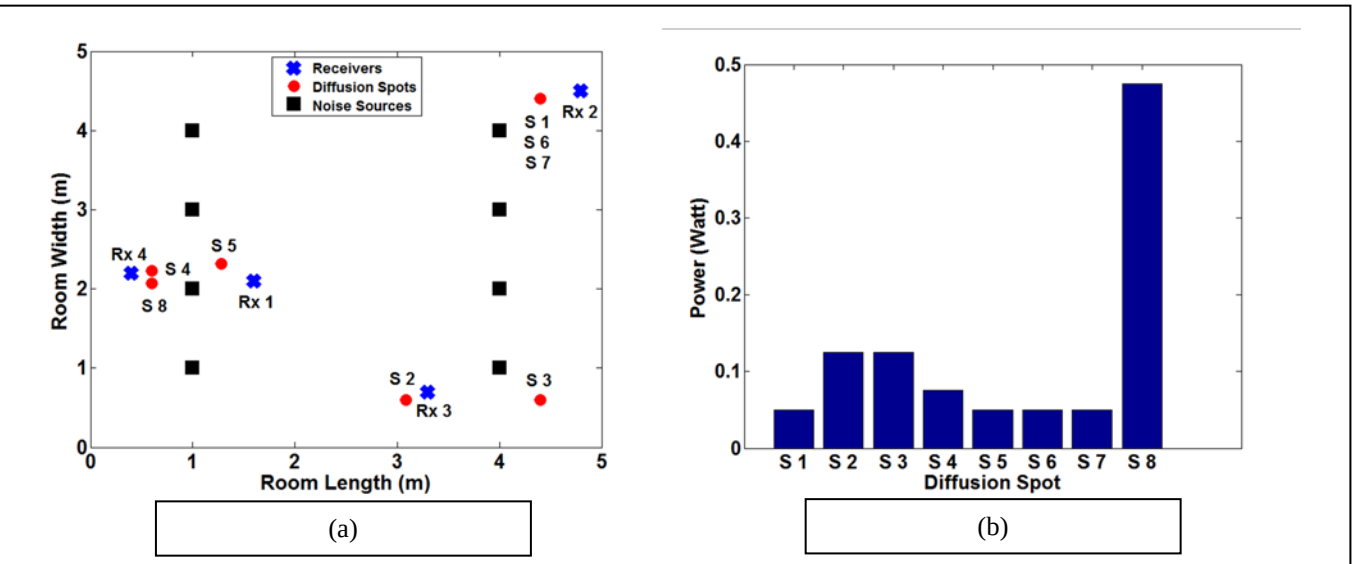

Fig. 4. Optimized parameters of diffuse spots for the second optimization scenario: (a) locations (top views), and (b) intensities of the diffusion spots scenario

TABLE 2. COMPARISON BETWEEN DIFFERENT OPTIMIZATION SCENARIOS

	Average SNR (dB)	Standard deviation of SNR	Average delay spread (sec)	Standard deviation of delay spread
Scenario A [14]	15.7580	3.3017	1.6630×10^{-9}	0.4364×10^{-9}
Scenario B [14]	17.5918	2.7129	1.3044×10^{-9}	0.6392×10^{-9}
Scenario 1	17.9881	3.5656	1.0270×10^{-9}	0.8462×10^{-9}
Scenario 2	19.4327	1.1508	0.9528×10^{-9}	0.5833×10^{-9}

power.

As shown in Figure 4(a), the locations of DiSs are distributed closer to the Rxs in order to ensure improved performance for the system. Both S2 and S3 are located close to Rx3, whereas S1, S6, and S7 are nearer to Rx2. S4, and S8 are located next to Rx4 and S5 is close to Rx1, which are also very close to the noise sources. In Figure 4(b), it is noted that the power level for S8 is high compared to other DiSs. This is because it serves Rx4 and is very close to the Rx1, and due to the fact that both Rxs are very close to the noise sources. Thus, S8 with higher intensity lead to high SNR values at Rxs1 and 4, which results in a more uniform SNR distribution for Rxs 1, 2, 3, and 4, see Table 2 and Figure 5 for more details.

Table 2 shows a comparison between the average SNR, the average delay spread, the standard deviation of SNR, and the standard deviation of delay spread for Scenarios 1 and 2, as well as Scenarios A and B for the centrally located position of DiSs with uniform power in [14] and the optimized distribution of DiSs using PSO in [14], respectively.

As shown in Table 2, optimization of position of the center of the DiSs' distribution (Scenario B with only location optimized) resulted in improvements in the average SNR and the standard deviation of SNR by 11% and 17%, respectively, and in the average DS by 21% compared to the centrally located position (Scenario A with no optimization). On the other hand Scenario A offers improved performance in terms of the standard deviation of DS. Optimization of locations and intensities of DiSs in Scenario 1 has resulted in improvement, in the average SNR and the average DS by 14% and 38%, respectively compared to Scenario A. On the other hand, the standard deviation of SNR and delay spread are better for Scenario A. For Scenario 2, optimization of locations and intensities of randomly distributed DiSs has resulted in improvement in the average SNR and the average DS by 23% and 42%, respectively, compared to Scenario A. The SNR standard deviation remarkably improved in Scenario 2 by 65% compared to Scenario A. The delay spread standard deviation in Scenario 2 is better than that in Scenarios B and 1, and only less than that in Scenario A. Note that, the increase in the average SNR and delay spread, and the SNR standard deviation in Scenario 2 is attributed to adopting more number of variables (i.e., 24 ins Scenario 2compared to 2 and 10 in Scenarios B and 1, respectively) in the optimization process, thus resulting in improved adaptability of DiSs to the environment being considered. This is best illustrated in Figure 4, where DiSs are distributed around the Rxs.

Since the delay spread values obtained satisfies the constraints on the maximum bit rate of 50 Mbps, we focus on SNR. Figure 5 depicts the bar chart for the maximum and minimum SNR values for all four scenarios. As shown in Figure 5, optimization in Scenario B shows an improved performance in terms of the minimum and the average SNR values. The decrease in difference between the SNR values contributed to improvment in SNR standard deviation, see Table 2. Scenario 1 outperforms Scenario A in terms of maximum minimum and average SNRs. The increase in the standard deviation in Table 2 can be related to the increase in the difference between maximum and minimum of SNR. For Scenario 2, we observe improvement in the average, the minimum, and the maximum SNRs, with maximum difference between SNR values of about 2.8 dB. Note that an equalization in the SNR performance is achieved, thus demonstrating the large increase in the SNR standard deviation, despite placement of the Rxs in different locations, with different degrees of degradation due to multipath propagation and noise It should be noted that in order to meet the eye safety requirements when selecting the maximum transmit power, there are a number of factors that must be considered, such as the number and the locations of the DiSs and the Lambertian reflection characteristics [10]. For the proof of concept we developed optimization based on the impulse response, however, in real practical systems the eye safety regulations must be considered.

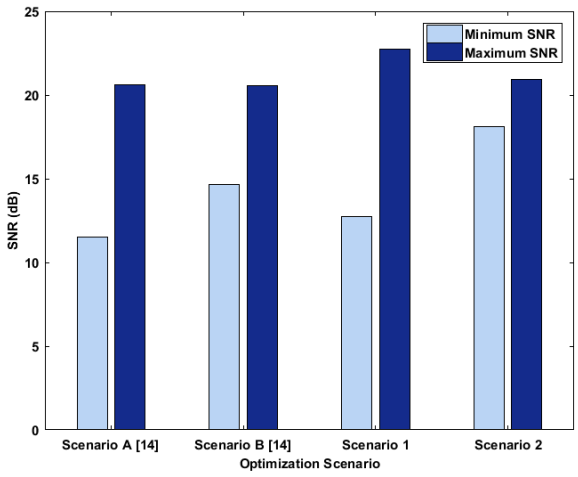

Fig. 5. Minimum and maximum SNR values achieved in each optimization scenario

Figure 6 illustrates the normalized fitness values versus the number of iterations for Scenarios 1, 2, and B [14]. It can be seen that Scenario 2 achieves higher fitness values compared to Scenario 1 beyond the iteration value of 6. In addition, Scenarios 1 and 2 outperform Scenario B [14] over all the iterations. This can be attributed to a higher number of variables being considered in the optimization process, i.e., more freedom for particles to achieve improved performance. Note that, for the same number of iterations, increasing the number of particles could improve the performance, but at the cost of increased computational time. The number of particles and iterations considered here are the same as in [14], in order to make comparison with the results of Scenarios A and B in [14].

To determine the changes in the SNR levels when the diffusion spots' locations are not fixed, simulations are carried out, accounting for up to 10% of diffusion spots' locations variations (i.e. error). Figure 7 shows achieved SNR values for different values of margin of error for the diffusion spots locations. As shown in Figure 7, for error values between -10% and 10%, the system had maximum variation for the SNR values of 0.9%, 10.3%, 3.4%, and 1.2% for Rx1, Rx2, Rx3, and Rx4, respectively. Note that, the 95% confidence interval for SNR for Scenarios 1 and 2 are bounded between 11.44 dB and 24.54 dB, and between 17.32 dB and 21.55 dB, respectively.

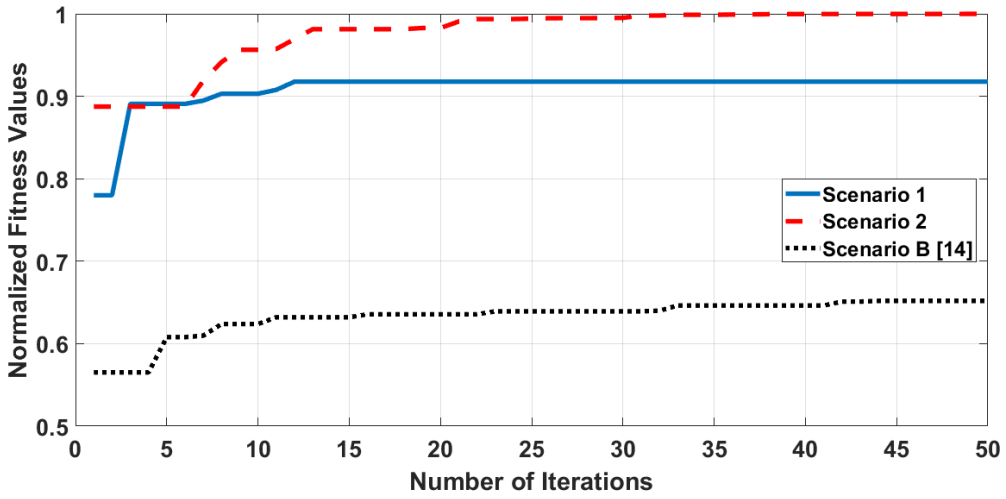

Fig. 6. Normalized fitness values versus iteration for Scenario 1, Scenario 2, and Scenario B [14].

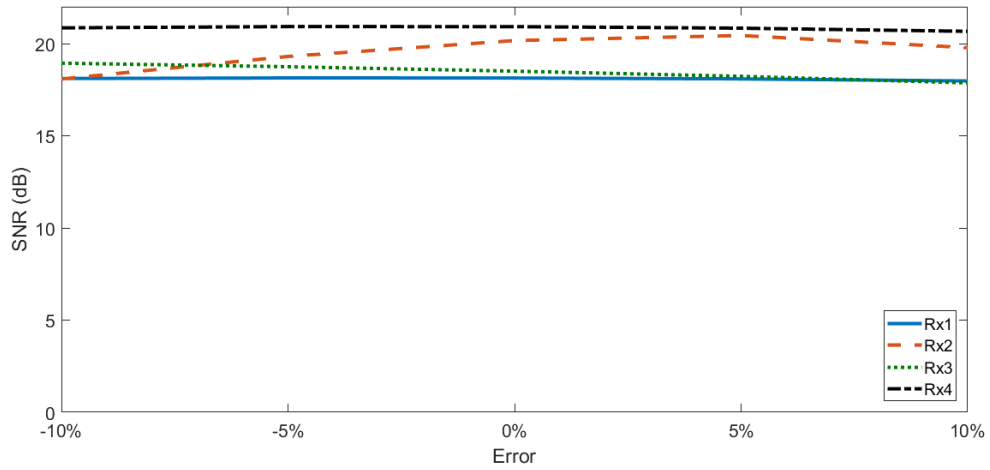

Fig. 7.SNR (dB) values at the Rxs in scenario 2 versus error percentage, for different values of margin of error for the locations of the diffuse spots

V. Conclusion

In this paper, optimization of locations and intensities of the diffusion spots in indoor OWC systems was carried out for maximizing and minimizing the SNR and the delay spread, respectively. Different optimization scenarios were considered, and were compared using different number of variables in terms of users' SNR and delay spread. We showed that there are up to 42% and 23% improvement achieved in Scenario 2 in the average delay spread and the average SNR, respectively. Also shown was the improvement in the standard deviation of SNR by up to 65% in the presences of the ambient lights' noise and multipath induced dispersion. We noted that increasing the number of variables in the optimization process allowed higher degrees of adaptability for diffuse spots within the communications environment, which resulted in improved performance.

References

[1] F. R. Gfeller and U. H. Bapst, "Wireless in-house data communication via diffuse infrared radiation," Proc. IEEE, vol. 67, no. 11, pp. 1474-1486, Nov. 1979.

[2] D. K. Borah, A. C. Boucouvalas, C. C. Davis, S. Hranilovic, and K. Yiannopoulos, "A review of communication-oriented optical wireless systems," EURASIP J. Wireless Commun. Netw., vol. 91, pp. 1-28, Apr. 2012.

[3] Ghassemlooy, Z., Alves, L. N., Zvanovec, S., and Khalighi, M-A.: Visible Light Communications: Theory and Applications, CRC June 2017.

[4] B. Mendoza, S. Rodrguez, R. Prez-Jimnez, A. Ayala and O. Gonzlez, "Comparison of Three Non-Imaging Angle-Diversity Receivers as Input Sensors of Nodes for Indoor Infrared Wireless Sensor Networks: Theory and Simulation", Sensors, vol. 16, no. 7, pp. 1086-1101, 2016.

[5] S. S. Torkestani, S. Sahuguede, A. Julien-Vergonjanne and J. P. Cances, "Indoor optical wireless system dedicated to healthcare application in a hospital," in IET Communications, vol. 6, no. 5, pp. 541-547, 2012.

[6] Z. Ghassemlooy, W. Popoola, S. Rajbhandari, Optical Wireless Communications: System and Channel Modelling with MATLAB, CRC Press, Boca 275 Raton, FL, USA, 2013.

[7] M. Uysal, C. Capsoni, Z. Ghassemlooy, A.C. Boucouvalas, E. G. Udvary (Eds.), Optical Wireless Communications - An Emerging Technology, Springer, 2016.

[8] J. M. Kahn and J. R. Barry, "Wireless infrared communications," Proc. IEEE, vol. 85, no. 2, pp. 265-298, Feb. 1997.

[9] J. R. Barry, J. M. Krause, E. A. Lee, and D. G. Messerschmitt, "Simulation of multipath impulse response for indoor wireless optical channels," IEEE J. Sel. Areas Commun., vol. 11, no. 3, pp. 367-379, Apr. 1993.

[10] M. D. Higgins, R. J. Green, and M. S. Leeson, "A genetic algorithm method for optical wireless channel control," J. Lightw. Technol., vol. 27, no. 6, pp. 760-772, Mar. 15, 2009.

[11] M. T. Alresheedi and J. M. H. Elmirghani, "Hologram selection in realistic indoor optical wireless systems with angle diversity receivers," IEEE J. Opt. Netw., vol. 7, no. 8, p. 797813, Aug. 2015.

[12] M. T. Alresheedi and J. M. H. Elmirghani, "High-Speed Indoor Optical Wireless Links Employing Fast Angle and Power Adaptive ComputerGenerated Holograms With Imaging Receivers," in IEEE Transactions on Communications, vol. 64, no. 4, pp. 1699-1710, April 2016.

[13] D. W. K. Wong, G. Chen, and J. Yao, "Optimization of spot pattern in indoor diffuse optical wireless local area networks," Opt. Express, vol. 13, no. 8, pp. 3000-3014, 2005.

[14] M. W. Eltokhey, K. R. Mahmoud, S. S. A. Obayya, Optimised di usion spots locations for simultaneous improvement in SNR and delay spread, Photonic Network Communications, 31 (2016), pp. 172-182.

[15] S. Jivkova, B. A. Hristov, and M. Kavehrad, "Power-efficient multispotdiffuse multiple-input-multiple-output approach to broad-band optical wireless communications," IEEE Trans. Veh. Technol., vol. 53, no. 3, pp. 882-889, May 2004.

[16] D. C. O'Brien, G. E. Faulkner, E. B. Zyambo, K. Jim, D. J. Edwards, P. Stavrinou, G. Parry, J. Bellon, M. J. Sibley, V. A. Lalithambika, V. M. Joyner, R. J. Samsudin, D. M. Holburn, and R. J. Mears, "Integrated transceivers for optical wireless communications," IEEE J. Sel. Topics Quantum Electron., vol. 11, no. 1, pp. 173-183, 2005

[17] J. M. Kahn, W. J. Krause, and J. B. Carruthers, "Experimental characterization of non-directed indoor infrared channels," IEEE Trans. Commun., vol. 43, no. 234, pp. 1613-1623, Apr. 1995.

[18] J. M. Kahn, J. R. Barry, M. D. Audeh, J. B. Carruthers, W. J. Krause, and G. W. Marsh, "Non-directed infrared links for high-capacity wireless LANs," IEEE Personal Commun., vol. 1, no. 2, pp. 12-25, Aug. 1994.

[19] J. M. H. Elmirghani, H. H. Chan, and R. A. Cryan, "Sensitivity evaluation of optical wireless PPM systems utilizing PIN-BJT receivers," IEE Proc. Optoelectron., vol. 143, no. 6, pp. 355-359, Dec. 1996

[20] A. G. Al-Ghamdi and J. M. H. Elmirghani, "Line strip spot-diffusing transmitter configuration for optical wireless systems influenced by background noise and multipath dispersion," IEEE Trans. Commun., vol. 52, no. 1, pp. 37-45, Mar. 2004

[21] J. Kennedy and R. Eberhart, "Particle swarm optimization," in Neural Networks, 1995. Proceedings., IEEE International Conference on Computational Intelligence, vol. 4, nov/dec 1995, pp. 1942-1948 vol.4.

[22] R. Hassan, B. Cohanim, O. de Weck, G. Venter, A comparison of particle swarm optimization and the genetic algorithm, in: 46th AIAA/ASME/ASCE/AHS/ASC Structures, Structural Dynamics and Materials Conference, 2005.

[23] E. Elbeltagi, T. Egazy, D. Grierson, Comparison among five evolutionary-based optimization algorithms, Adv. Eng. Inform. 19 (1) (2005), pp. 43-53.

[24] Y. Shi and R. C. Eberhart, ''A modified particle swarm optimizer,'' in Proc. IEEE Int. Conf. Evol. Comput., Anchorage, AK, USA, May 1998, pp. 69–73

[25] A. Ratnaweera, S. Halgamuge and H. Watson, "Self-Organizing Hierarchical Particle Swarm Optimizer With Time-Varying Acceleration Coefficients", IEEE Transactions on Evolutionary Computation, vol. 8, no. 3, pp. 240-255, 2004.

[26] M.B. Abdelhalim, S.E.D. Habib, Particle swarm optimization for HW/SW partitioning, in: Particle Swarm Optimization. In-Tech Publication, 2009, pp. 49-76, ISBN:978-953-7619-48-0.

[27] Hsun-Hung, C., Sterckx, K.L., Elmirghani, J.M.H., Cryan, R.A.: Performance of optical wireless OOK and PPM systems under the

constraints of ambient noise and multipath dispersion. IEEE Commun. Mag. 36(2), 83–87 (1998)

[28] S. S. Torkestani, Anne Julien-Vergonjanne, Jean-Pierre Cances, Mobile healthcare monitoring in hospital based on diffuse optical wireless technology, 2010 IEEE 21st International Symposium on In Personal Indoor and Mobile Radio Communications (PIMRC), pp. 1055-1059.

[29] Yan, X., He, F., Chen, Y., & Yuan, Z. (2015). An efficient improved particle swarm optimization based on prey behavior of fish schooling. Journal of Advanced Mechanical Design, Systems, and Manufacturing, 9(4), JAMDSM0048-JAMDSM0048.

[30] Turner, J. S., Ramli, M. F., Kamarudin, L. M., Zakaria, A., Shakaff, A. Y. M., Ndzi, D. L., ... & Mamduh, S. M. (2013, December). The study of human movement effect on Signal Strength for indoor WSN deployment. In Wireless Sensor (ICWISE), 2013 IEEE Conference on (pp. 30-35).